Supporting Information

Ultrathin GeSe Nanosheets: from Systematic Synthesis, to Studies of Carrier Dynamics and Applications for High Performance UV-Vis Photo-Detector

Dingtao Ma[†], Jinlai Zhao[†], Rui Wang[‡,§], Chenyang Xing[‡], Zhongjun Li[†], Weichun Huang[‡], Xiantao Jiang[‡], Zhinan Guo[‡], Zhengqian Luo[§], Yu Li[‡], Jianqing Li[†], Shaojuan Luo[‡], Yupeng Zhang[‡], and Han Zhang[‡*]*

† Faculty of Information Technology, Macau University of Science and Technology, Taipa, Macau SAR 999078, P. R. China

‡ Collaborative Innovation Center for Optoelectronic Science and Technology and Key Laboratory of Optoelectronic Devices and Systems of Ministry of Education and Guangdong Province, Shenzhen University, Shenzhen 518060, P. R. China

§ Department of Electronic Engineering, Xiamen University, Xiamen 361005, P. R. China

*Email: hzhang@szu.edu.cn; Email: ypzhang@szu.edu.cn

Solvent optimization for exfoliated GeSe nanosheets

The solvents, including NMP, DMF, water, ethanol and IPA, were used to exfoliate the bulk GeSe. For different solvents, the bulk GeSe was added in the same concentration of 1mg/ml. Then, all the mixtures were sonicated under the same condition. After exfoliation, they were centrifuged with a certain speed of 2000 rpm to get the supernatant and subsequent 14000 rpm to get the precipitate (denoted as 2-14 k hereafter). The received dispersion in different solvents were shown in Figure S1a. Then, the absorbance of the dispersions containing the exfoliated GeSe nanosheets were measured, as shown in Figure S1b. It was found that the GeSe nanosheets exfoliated in NMP solvent can obtain a much higher absorbance when compared with other counterparts, which demonstrates a better exfoliation result.

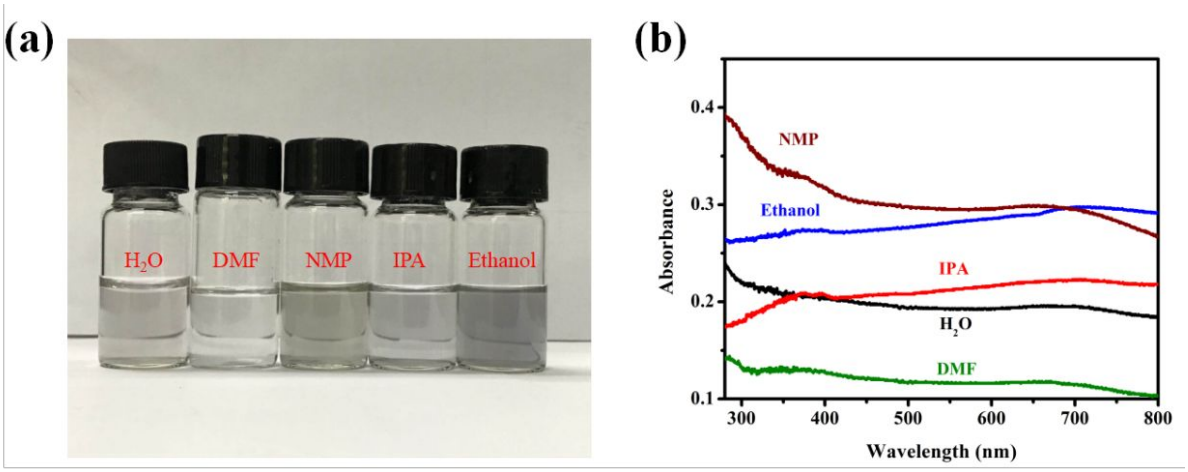

Figure S1. (a) The photograph for the different exfoliation effect of GeSe in different solvents. (b) The UV-vis absorbance tests for GeSe exfoliated in different solvents.

The effect of centrifugation speed on the thickness and size distribution of exfoliated GeSe nanosheets

To explore the effect of centrifugation speed on the thickness and size distribution of GeSe nanosheets, the fresh dispersions were subjected to centrifuge under different speed range, including 1000-14000 rpm, 2000-14000 rpm, and 3000-14000 rpm (denoted as 1-14 k, 2-14 k, and 3-14 k samples). For 1-14 k sample, the average thickness of 5.9 ± 0.1 nm could be detected for GeSe nanosheets (Figure S2a and S2b), while average thickness of 4.3±0.2 nm for 2-14 k sample (Figure 2c and 2d) and 3.04±0.06 nm for 3-14 k sample (Figure S2c and S2d), were found, respectively. In regard with the size distribution, the average lateral diameter would gradually decrease from 159 nm to 98 nm and 70 nm (Figure S3). Such results demonstrated that different thickness and size distributions of the GeSe nanosheets could be easily obtained by controlling the centrifugation speed.

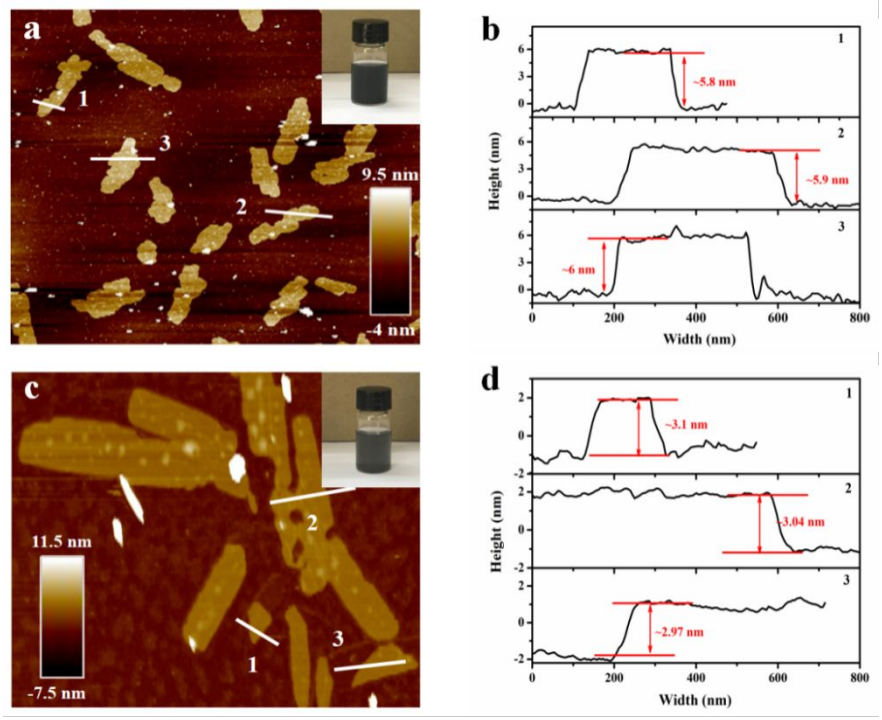

Figure S2. AFM images and the corresponding height profiles of the GeSe nanosheets obtained at a certain centrifugation speed of (a, b) 1-14 k, and (c, d) 3-14 k.

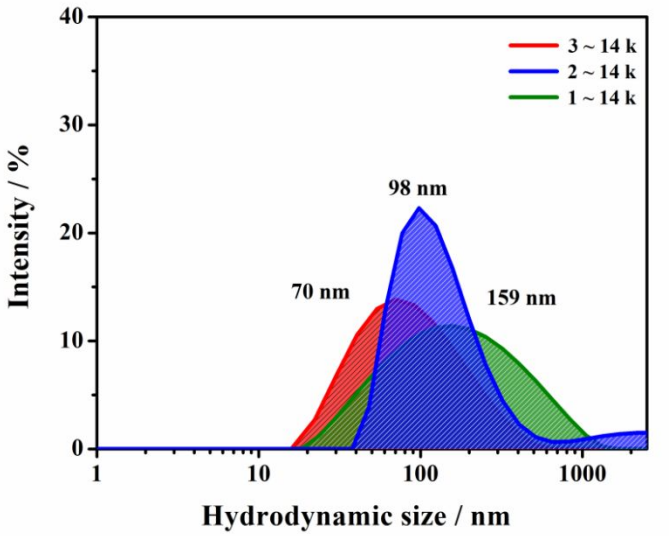

Figure S3. Size distributions of GeSe nanosheets obtained under various centrifugation.

The effect of thickness on the electrical and optical properties of exfoliated GeSe nanosheets

To explore the effect of thickness on the electrical and optical properties of GeSe nanosheets, the fresh dispersions were subjected to centrifuge under different speed range, including 1000-14000 rpm, 2000-14000 rpm, and 3000-14000 rpm (denoted as 1-14 k, 2-14 k, and 3-14 k samples). As indicated in Figure S2, different average thickness of GeSe nanosheets can be obtained with the increament of centrifugation speed, that is, 5.9 ± 0.1 nm for 1-14 k, 4.3±0.2 nm for 2-14 k, and 3.04±0.06 nm for 3-14 k, respectively. On this basis, the influence of thickness of GeSe nanosheets on the optical property can be estimated by comparing their corresponding UV-vis spectra. As shown in Figure S8, compared with the bulk GeSe, the GeSe nanosheets show a higher UV-vis absorption after exfoliation, especially the 3-14 k sample with the thinnest average thickness. This phenomenon indicates that the exfoliated GeSe nanosheets shows great

potential applied for UV-vis photodetector. While in terms of the studies concerning about the electrical property, the electrochemical impedence spectra (EIS) was employed to respectively test the charge transfer resistance (R_{ct}) of four different GeSe photoanodes contained the GeSe nanosheets mentioned above (Figure S9). Obviously, the exfoliated GeSe nanosheets exhibt a smaller R_{ct} than that of the bluk counterpart. Besides, it seems that the average thickness of GeSe shows a positive correlation with the R_{ct}. This might be resulted from the shorter electron transport path and higher carrier mobility of GeSe nanosheets after the exfoliated treatment.

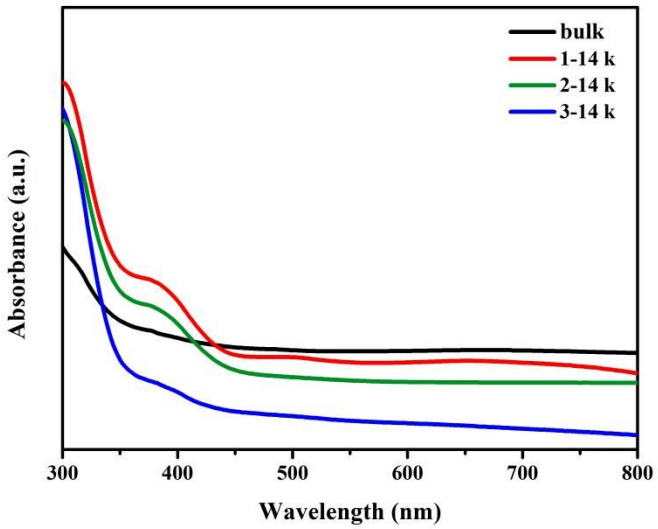

Figure S4. The UV-vis spectras of GeSe nanosheets obtained under various centrifugation conditions.

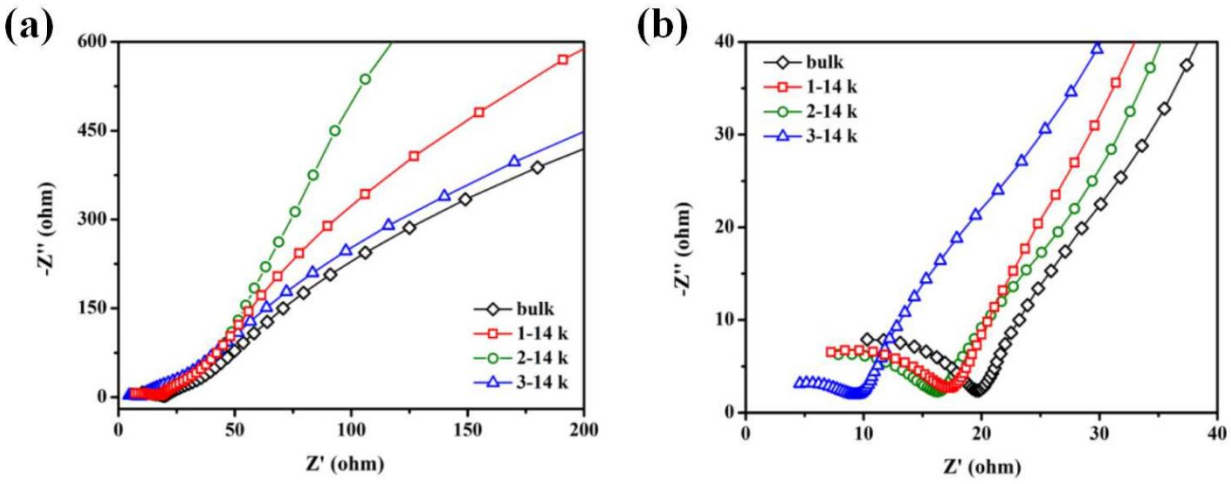

Figure S5. (a) The EIS results of GeSe nanosheets photoanodes and (b) the corresponding amplified plot, obtained under various centrifugation conditions.

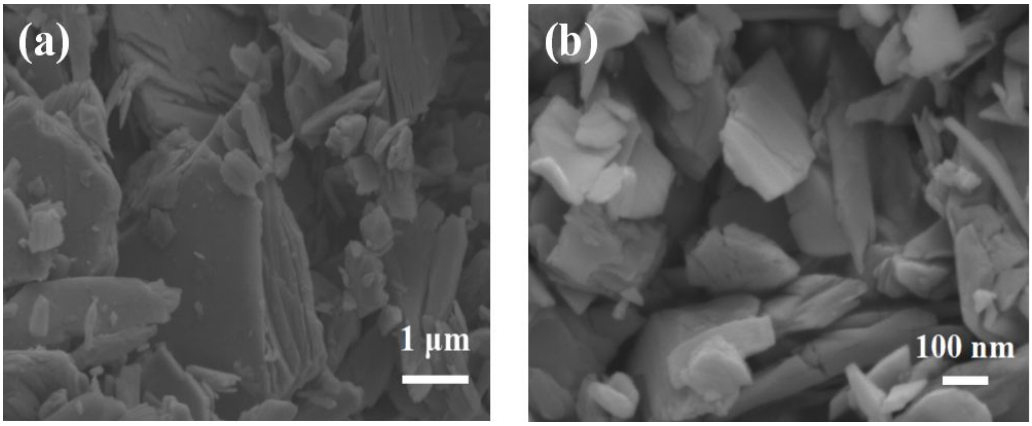

Figure S6. The FESEM images of (a) bulk GeSe and (b) GeSe nanosheets.

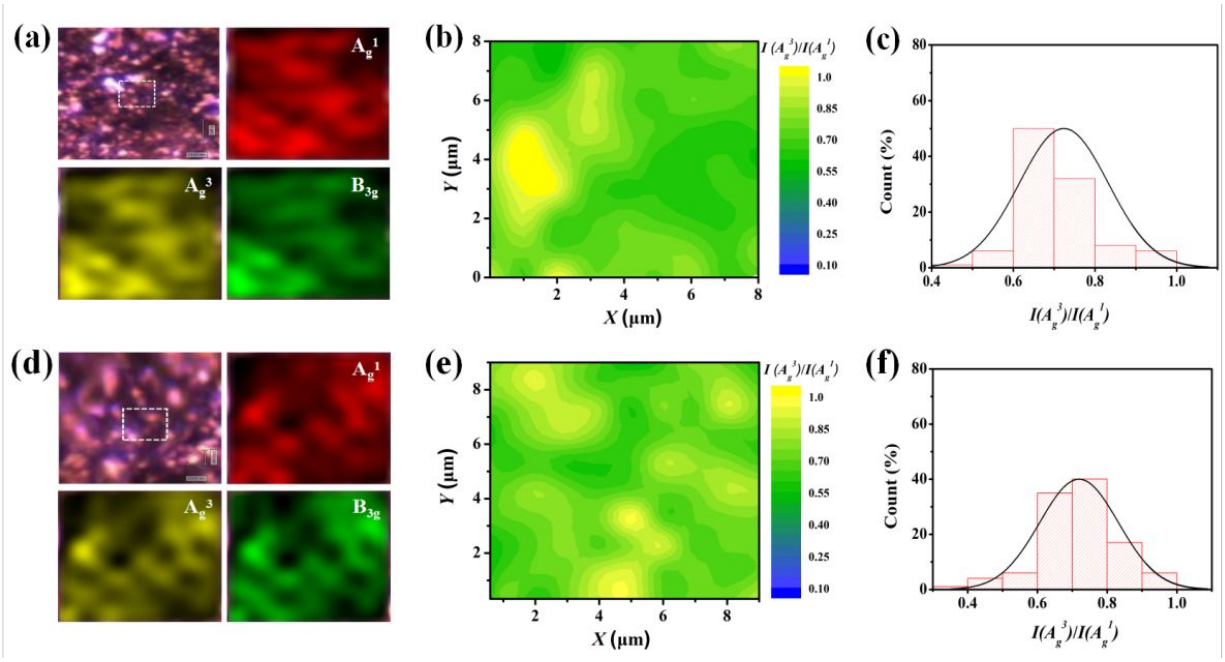

Figure S7. Raman mapping of A_g^1, B_{3g}, and A_g^3 models with the corresponding intensity ratio of $I(A_g^3)/I(A_g^1)$ for (a, b, c) GeSe nanosheets and (d, e, f) bulk GeSe.

Femtosceond transient optical absorption spectroscopy

This ultrafast system was utilized to study the carrier dynamics on the GeSe nanosheets. The pump light wavelength is 400 nm with the pulse duration of ~140 fs through a Ti: Sapphire femtosecond laser. The power of the pump light is tunable through a rotatable attenuator with a repetition rate of 500 Hz after pass through a chopper. In order to get high signal-to-noise TA absorption signal, we turned the pump power to 1mW, which is much larger than the power of the probe light. The probe light, (1 kHz, 500 nm to 650 nm), can automatic adjustment delay time between pump light through a delay device controlled by the computer. Eventually, probe light was overlapped with pump light on the sample, and the change in absorbance of the probe light ($\Delta A = -\log(I_{ex}/I_0)$) where I_0 and I_{ex} are the intensity of probe light after the sample without and with the pump light) were detected by spectrometer.

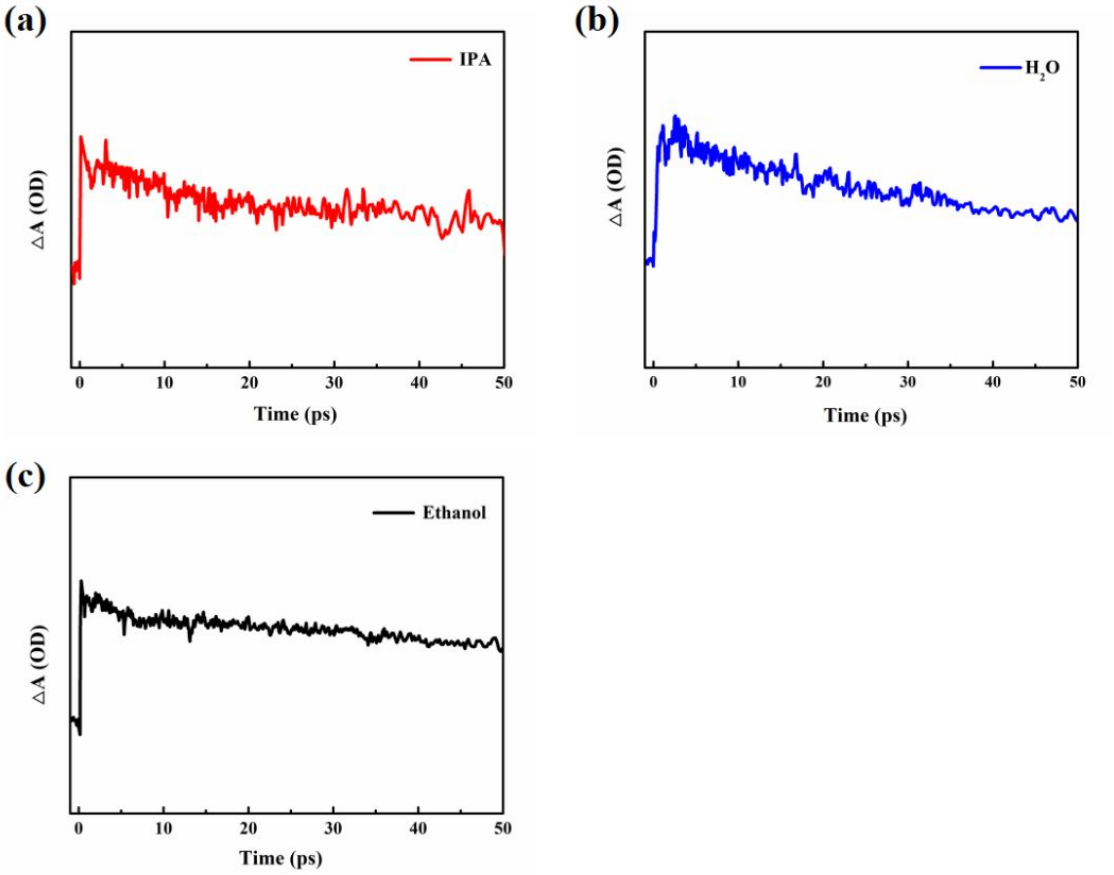

Figure S8. The kinetic curves of the GeSe nanosheets in various solution: (a) IPA, (b) H_2O, and (c) Ethanol.

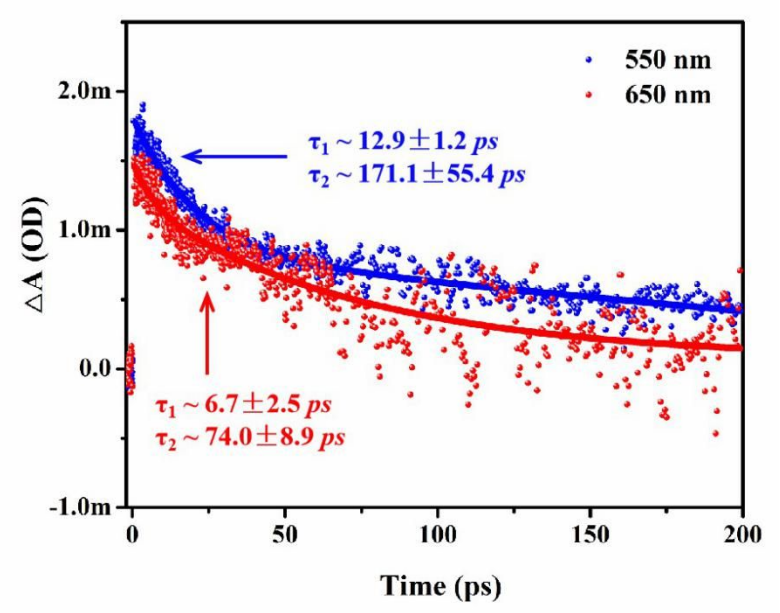

Figure S9. The kinetic curves and corresponding fitting results of the GeSe nanosheets in 550 and 650 nm of probe wavelengths.

To study the transition process of different energy carriers of the GeSe nanosheets, the kinetic curves were respectively measured at the probe wavelength of 550 and 650 nm. As can be seen in Figure S7, these two kinetic curves displayed a similar absorption decay tendency, indicating their similar carrier transition process. The corresponding fitting results imply that the carrier transfer process exist a fast and a slow component, both at the probe wavelength of 550 and 650 nm. Compared with the result tested at 550 nm (τ_1: 12.9 ± 1.2 ps; τ_2: 171.1 ± 55.4 ps), the GeSe nanosheets show a smaller τ1 (6.7 ± 2.5 ps) and τ2 (74.0 ± 8.9 ps) at the probe wavelength of 650 nm, indicating a faster recovery speed than that at 550 nm. Furthermore, the amplitude ratio of fast component at 550 and 650 nm are calculated to be ~ 56% and ~ 20%, respectively. This also reveals that the carrier recombination behavior dominates the carrier transfer process at 650 nm, owing to its high amplitude ratio (~80%) of the slow component.

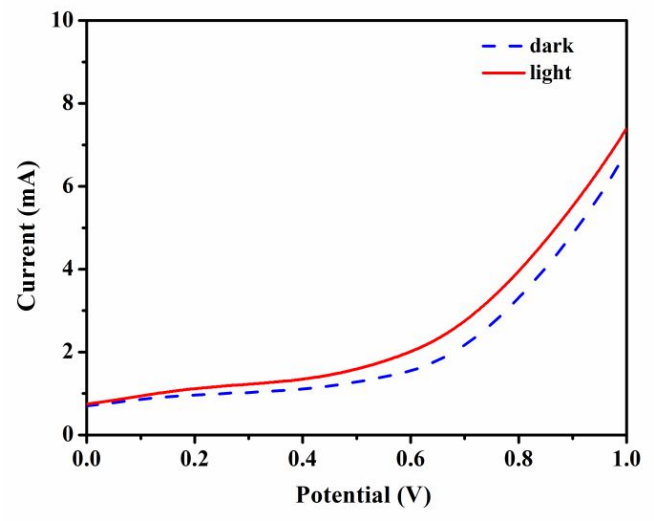

Figure S10. LSV measurements of the GeSe nanosheets under dark and light in 0.1 M KOH.

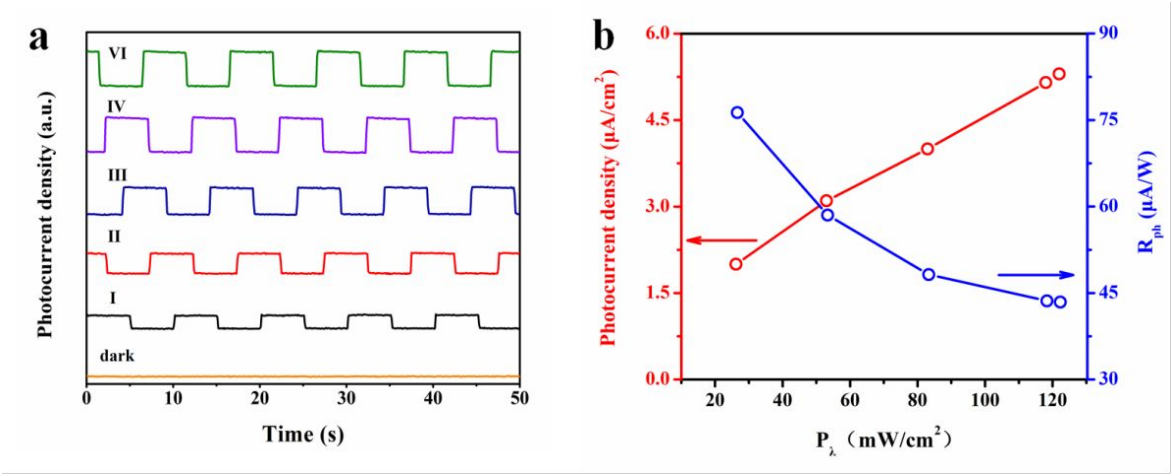

Figure S11. (a) On/off cylic stability tests under different various light power densities (levels I, II, III, IV and VI), in 0.1 M KOH electrolyte. (b) The calculated photoconversion efficiencies of GeSe nanosheets under various light power densities.

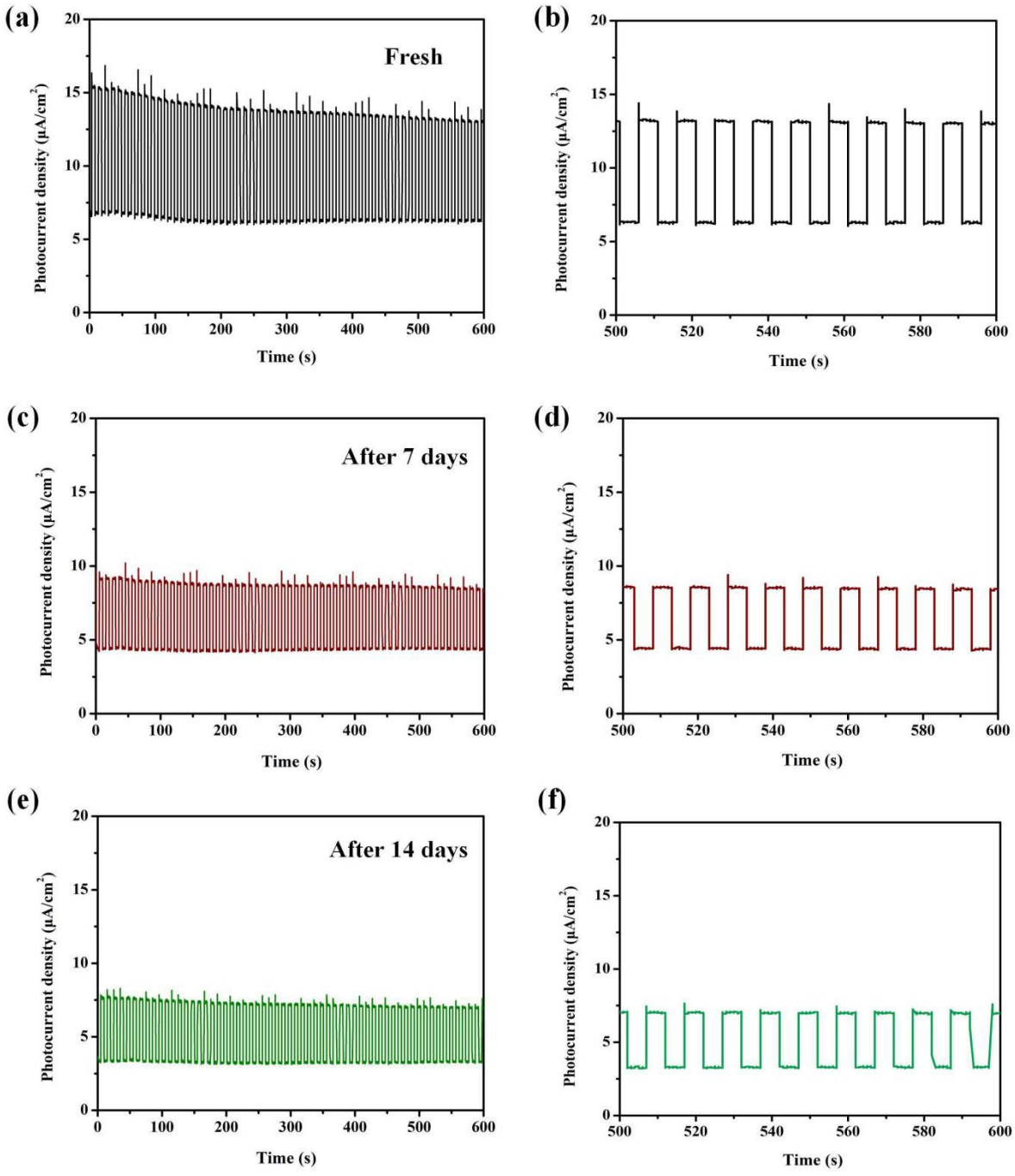

Figure S12. The stability of optoelectronic performances of GeSe nanosheets under illumination of simulated light after different storage periods: (a, b) fresh state; (c, d) after 7 days; and (e, f) after 14 days, under the illumination of simulated light at 0.6 V, in 0.1 M KOH electrolyte.

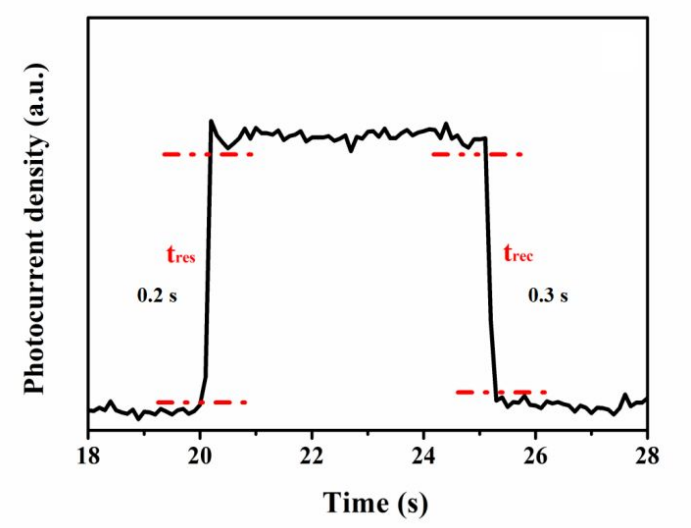

Figure S13. The profile of response time (t_{res}) and recovery time (t_{rec}) of the GeSe nanosheets based photodetector in 0.1 M KOH with bias potential of 0.3 V with the light power density of level IV (118 mW/cm^2).

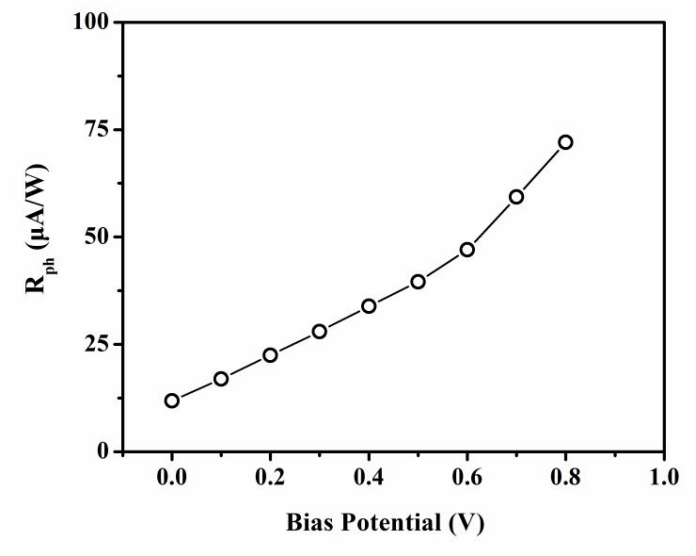

Figure S14. The calculated photoconversion efficiencies of GeSe nanosheets based photodetector under various external bias potential with the light power density of level IV (118 mW/cm^2).

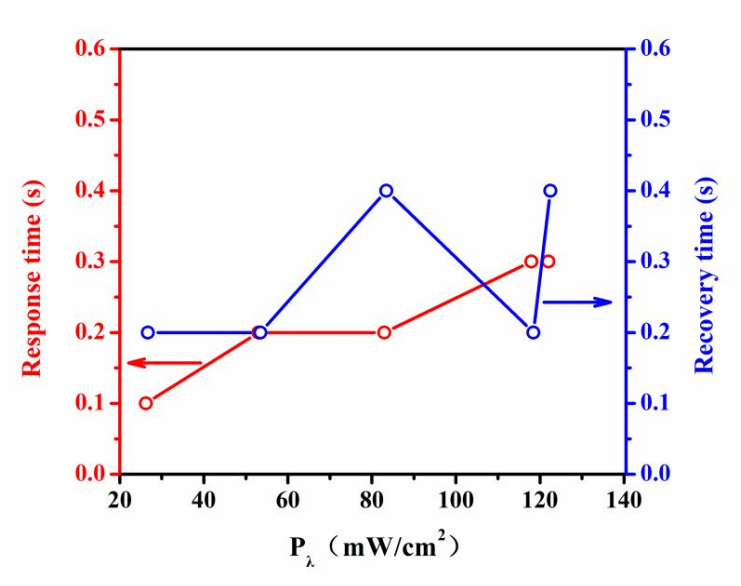

Figure S15. The profiles of response time (t_{res}) and recovery time (t_{rec}) of the GeSe nanosheets based photodetector in 0.5 M KOH electrolyte under different light power densities.

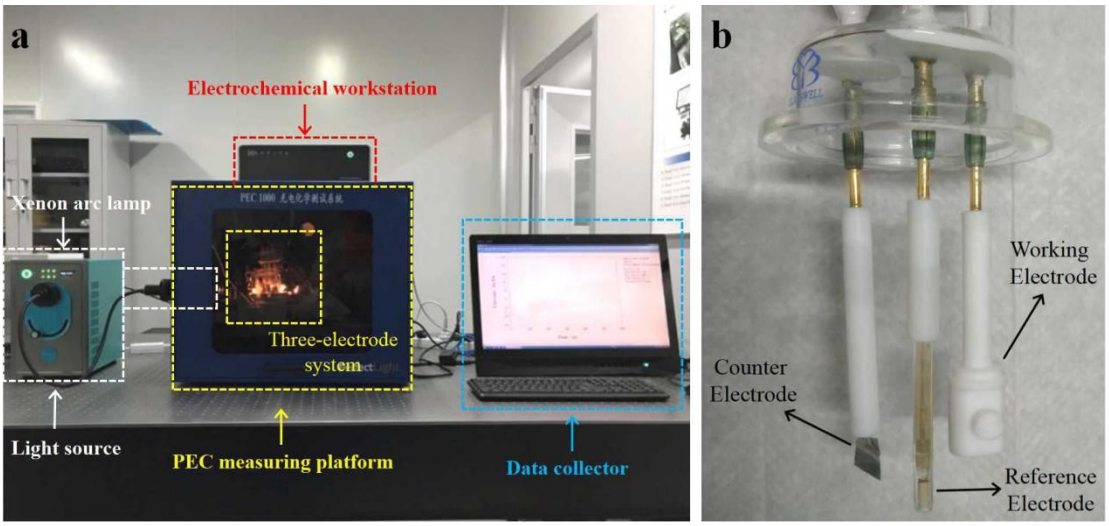

Figure S16. The digital photograph of (a) PEC-type photodetector device and (b) three-electrode system used in this work.

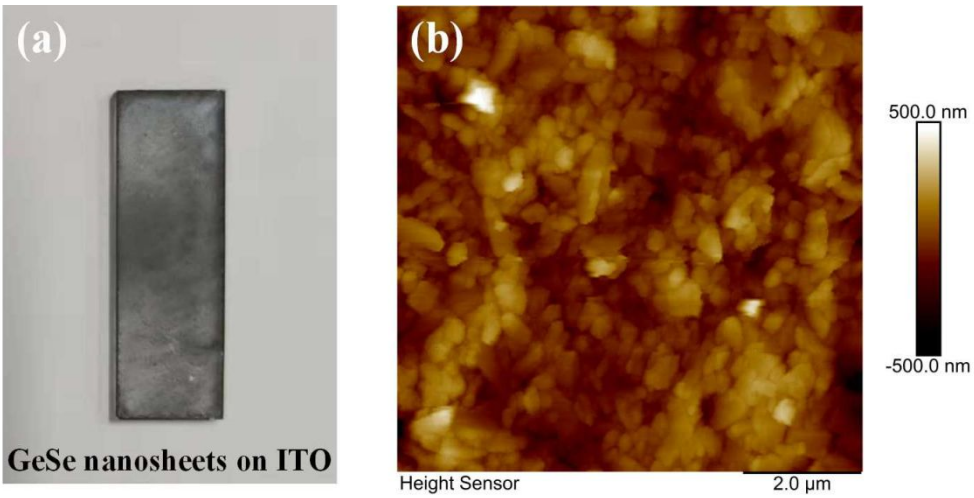

Figure S17. (a) The digital photograph of GeSe photoanode and (b) the corresponding AMF image.

Table S1. Typical parameters of ultrathin GeSe nanosheet-based photodetectors under various working conditions.

Wavelength [nm]	Working conditions	Light intensity [P_λ, mW·cm^{-2}]	Responsivity [R_{ph}, μA·W^{-1}]	Detectivity [D^*, Jones]	EQE [%]
Simulated light	0.3 V, 0.1 M KOH	26.2	76.3	1.3×10^{11}	—
		53	57.4	9.7×10^{10}	—
		83.1	48.1	7.06×10^{10}	—
		118	43.6	6.28×10^{10}	—
350	0.3 V, 0.5 M KOH	2.17	2304	2.1×10^{12}	816
365		3.57	294.1	3.7×10^{11}	102
380		2.68	304.1	4.3×10^{11}	98

400		5.22	173.4	2.2×10^{11}	54
475		10.1	78.2	1.04×10^{11}	20
550		8.28	24.7	4.0×10^{10}	5.6
650		8.54	18.7	3.14×10^{10}	4.2

Table S2. The power densities (P_λ) of incident light with various irradiation wavelengths. The gradually increased P_λ were labelled with I, II, III, IV, and VI levels, respectively.

Light / P_λ	*I* (mW/cm^2)	*II* (mW/cm^2)	*III* (mW/cm^2)	*IV* (mW/cm^2)	*VI* (mW/cm^2)
Simulated light	26.2 ± 0.02	53.0 ± 0.01	83.1 ± 0.02	118.0 ± 0.02	122.0 ± 0.02
350 nm	0.51 ± 0.03	1.02 ± 0.01	1.66 ± 0.02	2.17 ± 0.02	2.19 ± 0.01
365 nm	0.76 ± 0.01	1.66 ± 0.04	2.55 ± 0.02	3.57 ± 0.02	3.69 ± 0.03
380 nm	0.32 ± 0.02	1.02 ± 0.01	1.91 ± 0.04	2.68 ± 0.02	2.77 ± 0.03
400 nm	0.64 ± 0.03	2.04 ± 0.02	3.57 ± 0.04	5.22 ± 0.02	5.35 ± 0.02
475 nm	1.91 ± 0.02	4.33 ± 0.02	7.01 ± 0.03	10.1 ± 0.03	10.6 ± 0.02

550 nm	2.04 ± 0.01	3.95 ± 0.01	5.98 ± 0.02	8.28 ± 0.04	8.40 ± 0.03
650 nm	2.04 ± 0.02	4.08 ± 0.03	6.02 ± 0.01	8.54 ± 0.03	8.92 ± 0.02